Theoretical Study of the Absorption Spectrum of $[(NH_3)_5Ru-(4,4'\text{-bipyridine})]^{2+}$ in Solution

Ivo Cacelli[†] **and Alessandro Ferretti***[,‡]

Scuola Normale Superiore, Piazza dei Cavalieri, I-56126 Pisa, Italy, and Istituto di Chimica Quantistica ed Energetica Molecolare and MITER del CNR, Via Risorgimento 35, I-56126 Pisa, Italy

Received: February 9, 1999; In Final Form: April 16, 1999

The absorption spectrum of $[(NH_3)_5Ru-(4,4'\text{-bipyridine})]^{2+}$ in the visible has been studied by ab initio methods, taking into account solvent effects by means of the polarizable continuum model and performing extensive CI calculations. The dependence of the ground and lowest excited states has been investigated as a function of the torsional angle between the two pyridine rings of bipyridine in vacuo, as well as in nitromethane, water, and dimethylsulfoxide. Including the torsion, the position and profile of the metal-to-ligand charge transfer band has also been computed. The results obtained in water are in good agreement with the only experimental result available, while they are predictive in the two other solvents.

Introduction

In recent years, organometallic compounds made by transition metals with N−aromatic ligands have drawn the interest of both experimentalists and theoreticians from various fields. In fact, such compounds are the basic units of more extended systems that are investigated for the study of intramolecular electron and energy transfer and their related properties.[1]

Ru compounds, with bidentate ligands such as pyrazine (pyz) or 4,4′-bipyridine (bpy) and many others,[2] are among the favorites. In fact, they can have very low and intense electronic excitations and thus be highly polarizable, which translates into significant conductive[3] and nonlinear optical properties,[4] especially when the metal atoms are in different oxidation states (mixed-valent compounds). These materials are therefore of interest for possible applications in molecular electronic devices, and from this perspective, it is worthwhile to reach a good understanding of the properties of their building blocks, which may serve well when designing materials with given properties.

For extended systems with several metal−ligand units, the only theoretical possibility is to build simplified models that, including the relevant physics, allow the understanding of specific properties.[4−8] However, the single units can be studied by performing extensive ab initio calculations[9] that, besides a solid theoretical knowledge of the units themselves, can also furnish useful insights for building simplified models for the corresponding extended systems.

One of the possible candidates for such a study is $[(NH_3)_5\text{-}Ru-(4,4'\text{-byp})]^{2+}$ (Figure 1), which is the subject of the present work. This is an interesting compound, being part of the well-known partially localized bpy-bridged Ru dimer, which has been recently modeled with a four-orbital two-band Hubbard Hamiltonian.[6] The model predicts that the weak band at ∼1 eV observed for the mixed-valent species (one Ru(II) and one Ru(III)) is a metal-to-ligand charge transfer (MLCT), in contrast with the commonly accepted assignment assessing that it is an intervalence, or metal-to-metal charge transfer.[10] Although Raman experiments[11] are clearly in favor of an MLCT assignment, showing that resonance enhancement occurs even for the Ru(II)−Ru(II) system and that the vibrational ladder of ligand modes appears, there is still no definitive answer. From this perspective, the results of ab initio calculations are of fundamental importance. However, before attacking the large Ru dimer, we first want to study carefully the moiety $[(NH_3)_5Ru-(4,4'\text{-byp})]^{2+}$.

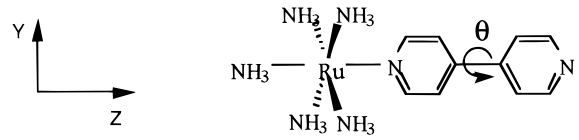

Figure 1.

In a previous paper[9] we have studied the smaller $[(NH_3)_5\text{-}Ru\text{-}pyz]^{2+}$ ion by performing extensive CI calculations and including solvent effects by using the well-known polarizable continuum model (PCM) by Tomasi and coworkers.[12] We have found that only a suitable inclusion of solvent effects allows a good agreement between theoretical predictions and experiments, at least as far as the near-IR−visible optical properties are concerned. In particular, we have been able to contribute to the theoretical understanding of the energy shift, observed experimentally changing the solvent, of the MLCT transition (solvatochromic effect), a problem that has been widely investigated in the literature.[13−15]

Here, we want to apply the same method to the 4,4′-bpy compound. This ion has not been studied extensively in various solvents as its pyz companion,[16] and only data in water are available[17] (data are instead available for the N−Me analogue[18]). From this perspective our computations thus also have a predictive character.

The compound 4,4′-bpy has two rings connected by a C−C single bond that can rotate relative to each other and thus change the interaction of the π orbitals of the two rings, i.e., their delocalization. The torsion can then be expected to play a significant role in determining the observed solvatochromic effect on the low-energy absorption, both in the ion studied here and in the most studied bridged Ru dimer.[16,19] For this reason, in the present paper we have carried out an accurate study of

[†] Scuola Normale Superiore. E-mail: ivo@hal.icqem.pi.cnr.it.
[‡] Istituto di Chimica Quantistica ed Energetica Molecolare and MITER del CNR. E-mail: profin@ibm580.icqem.pi.cnr.it.

10.1021/jp990489m CCC: $18.00
Published on Web 05/20/1999

the MLCT transition in various solvents, as well as of the dependence of the involved states on the ring−ring torsional angle.

Method and Computational Details

The study reported in the present paper has been performed by extensive CI calculations in which the solvent is taken into account by the PCM approach.[12] This method, as well as all others derived from the Onsager reaction field model,[20] sees the solute molecule surrounded by a cavity, which is the interface with the solvent represented as a polarizable continuum medium with dielectric constant ϵ. The solvent, polarized by the solute molecule, gives rise to a charge distribution on the cavity surface that generates a reaction field potential $W(\rho_a,\epsilon,\Omega)$ that must be added to the solute electrostatic Hamiltonian in a vacuum, H_0. For a fixed nuclear configuration of the solute, one then has to solve the following eigenvalue problem:

$$(H_0 + W(\rho_a,\epsilon,\Omega))|\psi_a\rangle = V_a|\psi_a\rangle \quad (1)$$

where ρ_a is the electronic + nuclear charge density of the ath state (ψ_a) of the solute and Ω represents the general dependence on the shape and size of the cavity. Once ρ_a is given, the surface density charge is found by imposing definite boundary conditions at the cavity surface,[21] derived by classical electrostatics.

This approach in principle should be modified when dealing with electronic excitations. In fact, under a sudden excitation from the ground to the ath state, the solvent does not have the time to relax to reach equilibrium with the new electronic density ρ_a. The corresponding nonequilibrium problem can be solved in a semiclassical picture, partitioning the solvent susceptibility into two terms, χ_{slow} and χ_{fast},[22−25] respectively related to the nuclear and electronic relaxation times. However, since we have found previously[9] that this heavy procedure affects negligibly the transition energies, we have solved the simplified version of eq 1:

$$(H_0 + W(\rho_0,\epsilon,\Omega))|\psi_a\rangle = V_a|\psi_a\rangle \quad (2)$$

taking into account only the reaction field in equilibrium with the ground-state ψ_0.

In the PCM calculations reported here it is very important that the cavity be properly chosen. In fact, owing to the +2 charge and to formation of ammonia−solvent hydrogen bonds for the compound under study, solvent effects are expected to be very strong. In principle, the hydrogen bond cannot be properly treated by the PCM, which is based on classical arguments. However, if one is interested in a good representation of the electronic density far enough from the solute−solvent interaction surface, this problem can be overcome with a proper choice of the shape and dimension of the cavity. This has been done by us[9] for the $Ru(NH_3)_5$ fragment, which can form hydrogen bonds with the solvent. Since the ligand bpy does not alter appreciably the NH_3−solvent interaction, the cavities optimized in ref 9 can be utilized here without changes. While the details of the method can be found in ref 9, we only briefly mention here the basic outlines as a reminder.

We want to build an optimal cavity for the $Ru(NH_3)_5$ fragment by means of one sphere centered on each ammonia nitrogen. Taking as a prototype species for $[Ru(NH_3)_5L]^{+2}$ the simplified ion $[RuHe_5NH_3]^{2+}$, we have performed two types of calculation for each of the three solvents considered: nitromethane (NM), water, and dimethylsulfoxide (DMSO). For a supermolecule in which three real solvent molecules are appropriately placed along the N−H bond directions, we have computed the SCF-HF electron density (ρ_S) in the Ru−N−H-solvent region. The same quantity has been computed at the SCF level with the PCM (ρ_{PCM}) at various values of the radius of the sphere on the ammonia, and the optimal radius has then been taken as that giving $\rho_{PCM} \approx \rho_s$ in the Ru−N region. The results obtained are summarized in Table 1 (see also ref 9), and the R_{PCM} values reported are those that have been utilized for the five ammonia molecules of $[(NH_3)_5Ru-(4,4'\text{-byp})]^{2+}$ in the computation with the solvent. The extension of the results obtained for the prototype ion $[He_5RuNH_3]^{2+}$ to the complex under study is based on the assumption that the ligand field on the metal is the sum of independent contributions coming from each NH_3. This is very reasonable because of the nearly electrostatic nature of the Ru−NH_3 bond. Again, we want to stress that the criterion proposed for obtaining the best cavity may be successfully employed, since the region of space relevant for MLCT transitions is far enough from the H-bonded solute−solvent interface.

TABLE 1: Optimized Radius of the Sphere on NH_3 in PCM Calculations[9]

solvent	DN[a]	ϵ[b]	R_{PCM}[c] (Å)
NM	2.7	38.2	1.82
H_2O	18.1	78.4	1.72
DMSO	29.8	46.7	1.67

[a] Donor number. [b] Dielectric constant at 25 °C. [c] Optimized radius of the spheres surrounding ammonia in PCM calculations.

As far as the cavity surrounding the bpy ligand molecule is concerned, we have made some changes in comparison with our previous study, where we took a single sphere for the whole pyz ring. To have a more appropriate shape of the cavity surrounding 4,4′-bpy rings, we have here taken one sphere for each C−H of the ring (R = 1.78 Å) centered in the middle of the C−H bond plus a sphere on the center of the ring (R = 2.90 Å). The cavity on the bpy is the same for each solvent.

Since we are interested in the study of the ion as the torsional angle θ varies, for each value of θ considered we have optimized in vacuum all the remaining ligand degrees of freedom (the fragment $Ru(NH_3)_5$− has been kept fixed at the same geometry as in the pyz compound), performing density functional calculations based on the three-parameter Becke functional (B3LYP).[26] The optimized geometries in vacuum have then been utilized also for the calculations in solution. In all calculations the 6-31G basis and the 36-electron ECP of Hay and Wadt[27] with the corresponding DZ basis set for Ru have been used.

The next step we have carried out is a PCM-SCF-HF calculation to obtain an approximate ψ_0 (and ρ_0). The integrals have then been transformed from an atomic to a molecular basis, including the one-electron reaction field matrix in equilibrium with the SCF ground-state density. In this step we have frozen 28 orbitals and considered the subspace generated by the remaining 41 occupied MO's plus the lowest 41 virtual MO's. These 82 orbitals have been considered in the multireference CI calculations in which the configuration space is gradually enlarged step by step according to the so-called aimed selection.[28] Each step involves the following actions.

(i) Once given a configurational space S_0, the lowest eigensolutions (four in the present case) are computed by standard methods. These are called zero-order states.

(ii) The first-order perturbative contribution to the zero-order states, which arises from single and double excitations from all detors belonging to S_0, is computed. The new space obtained by S_0 plus its single and double excitations is called perturbative space S_p.

TABLE 2: MLCT ($d_{xz} \rightarrow \pi^*$) Excitation Energy (E_{MLCT}) in H_2O at $\theta = 0°$ [a]

calculation type	E_{MLCT} (eV)
$\Delta\epsilon - J + 2K$	4
CI-V ($\eta = 0.34$, $D = 87$)	3.2
CI-V ($\eta = 0.32$, $D = 174$)	2.69
CI-V ($\eta = 0.17$, $D = 4860$)	2.64
CI-V ($\eta = 0.12$, $D = 26500$)	2.66
CI-VP (from $\eta = 0.17$)	2.40

[a] $\Delta\epsilon$ is the difference of orbital energies, and D is the dimension of the configurational space.

(iii) A subspace S_η of S_p is selected so that the norm of the first-order correction to the zero-order states is equal to a given value η. Note that η is the same for all the desired states (four here) and for all the geometries considered. This is the key point of the method.

(iv) The configurational space S_η is added to S_0, giving rise to the new variational space to be used in the next step. If the dimension of the space ($S_0 + S_\eta$) is large enough, the lowest eigensolutions are computed and the sequence stopped. In the other case the value of η is decreased and the procedure restarts from step i.

This method of selection of the configurational space guarantees that the final eigensolutions all have the same quality controlled by η. The dimension of the final space depends on the geometry (θ in the present case), which is of relevance when one wants to get balanced energies both for different geometries (e.g., for various values of θ) and for different states. This is therefore a valid alternative approach to the more standard MR-CI in which the configurational space is fixed.

The variational calculations (CI-V) that we report here ranges from 20 000 and 40 000 detors depending on θ and are obtained by a final value of $\eta = 0.12$. For example, in the case of water as solvent and for $\theta = 0°$ this space has dimension 26 500 and includes 674, 11 608, 13 844, 357, and 16 first, second, third, fourth, and fifth excited detors, respectively.

A second type of calculation, the variational-perturbative (CI-VP), is based on the second-order diagrammatic perturbation;[28] the ($S_0 + S_\eta$) space obtained by $\eta = 0.17$ ($\sim$7000 detors) is considered for obtaining zero-order states. The second-order energy corrections by the contribution of single and double excitation of all detors belonging to the ($S_0 + S_\eta$) space are then included in the final energies.

It is worthwhile to stress that our CI-VP energies include the contributions of $\sim 10^{10}$ detors and make the results stable with respect to the choice of the SCF orbitals. For instance, starting from an SCF in which suitable Nesbet occupation numbers are used to perform a pseudo-state-averaged calculation, the excitation energies change by no more than 0.03 eV.

To give further elements for an estimate of the accuracy of our calculations (see also Tables 3 and 4 of ref 9), we report in Table 2 the results obtained in the various steps for the MLCT ($d_{xz} \rightarrow \pi^*$) excitation energy in water at $\theta = 0°$. It is evident that a good stability of the excitation energy versus the CI space dimension is reached in the CI-V calculations and that the perturbative correction is small enough ($\sim$0.25 eV) to let us be confident to have a final accuracy of our results of less than 0.1 eV.

The torsional degree of freedom wave functions are computed in the Born−Oppenheimer approximation by projecting the corresponding eigenvalue problem (in au)

$$\left[-\frac{1}{2I_R}\frac{d^2}{d\theta^2} + V_a(\theta)\right]\chi_{ja}(\theta) = E_{ja}\chi_{ja}(\theta) \qquad (3)$$

on a large basis of trigonometric $\cos(k\theta)$ and $\sin(k\theta)$ functions. V_a is the energy of the electronic state ψ_a (eq 2). Considering free rotation between the group of five NH_3's and the pyr ring close to Ru, the moment of inertia I_R can be taken as the reduced moment of inertia of the two rings with respect to the Ru−N−C−C−N axis ($I_R \approx 43$ amu Å^2). The quantum photoabsorption cross section (σ_Q) is then computed taking into account the statistical population, at room temperature, of the torsional levels of the electronic ground state by

$$\sigma_Q(\omega) = \frac{2\pi^2}{cZ_Q}\sum_{j,m} e^{-E_{j0}/(k_B T)}\, f(m1 \leftarrow j0)\, \delta(\omega - E_{m1} + E_{j0}) \qquad (4)$$

where E_{j0} and E_{m1} are the energies of the rotational states of the electronic ground ψ_0 and excited state ψ_1, respectively, c the speed of light, and δ the Dirac delta function. Z_Q is the quantum partition function of the internal torsion coordinate ($Z_Q = \sum_j e^{-E_{j0}/(k_B T)}$). The oscillator strength $f(m1 \leftarrow j0)$ is, in the dipole-length approximation,

$$f(m1 \leftarrow j0) = \frac{2}{3}(E_{m1} - E_{j0})\left|\int d\theta\, \chi^*_{j0}(\theta)\, T_{01}(\theta)\, \chi_{m1}(\theta)\right|^2 \qquad (5)$$

where T_{01} is the electronic transition moment between the two electronic states in the dipole approximation.

The discrete function of eq 4 only takes into account the vibronic contribution due to the torsion. The effect of the other nuclear degrees of freedom, which is also of importance, is not considered here, since it would require an extensive study of the ground and excited potential energy surfaces. To mimic these effects and obtain a line shape profile, we have convoluted the cross section of eq 4 with a Gaussian function of fwhm = 0.1 eV.

In light of the small variation of the energy with θ, the classical statistical cross section

$$\sigma_c(\omega) = \frac{4\pi^2}{3cZ_c}\int d\theta\, e^{-V_0(\theta)/(k_B T)}|T_{01}(\theta)|^2[V_1(\theta) - V_0(\theta)]\, \delta[\omega - V_1(\theta) + V_0(\theta)] \qquad (6)$$

may provide a simplified and accurate enough expression for the photoabsorption intensity. Z_c is here the classical partition function of the electronic ground state. Since T_{01} does not change much with θ, the above integral may be easily and accurately computed by numerical quadrature. However, the results obtained by eq 6 are about the same as those obtained by the quantum expression 4.

Results and Discussions

In the complex under study, as for the pyz compound, Ru(II) has a low-spin $4d^6$ configuration. The bpy breaks the octahedral symmetry at the Ru atom and removes the degeneracy of the t_{2g} orbitals of Ru. Taking the pyridine (pyr) ring of 4,4′-bpy bound to Ru in the *yz* plane, with the Ru−Npyr (Npyr is the N of pyr) on the *z* axis, the highest occupied metal orbitals involved in the low-energy excitations are $4d_{xz}$, $4d_{x^2-y^2}$, and $4d_{yz}$. For the ligand, relevant orbitals are the two π^*'s resulting from the pyr π^*'s that have mainly N character, one on each pyr ring of bpy. This can be seen in the maps (in water), reported in Figures 2 and 3, of the HOMO and the two lowest π^*'s. When the two pyr rings are perpendicular ($\theta = 90°$; Figure 2), the HOMO is practically the Ru d_{xz}, with a small charge on the first ligand ring, the LUMO is essentially the π^* on the pyr

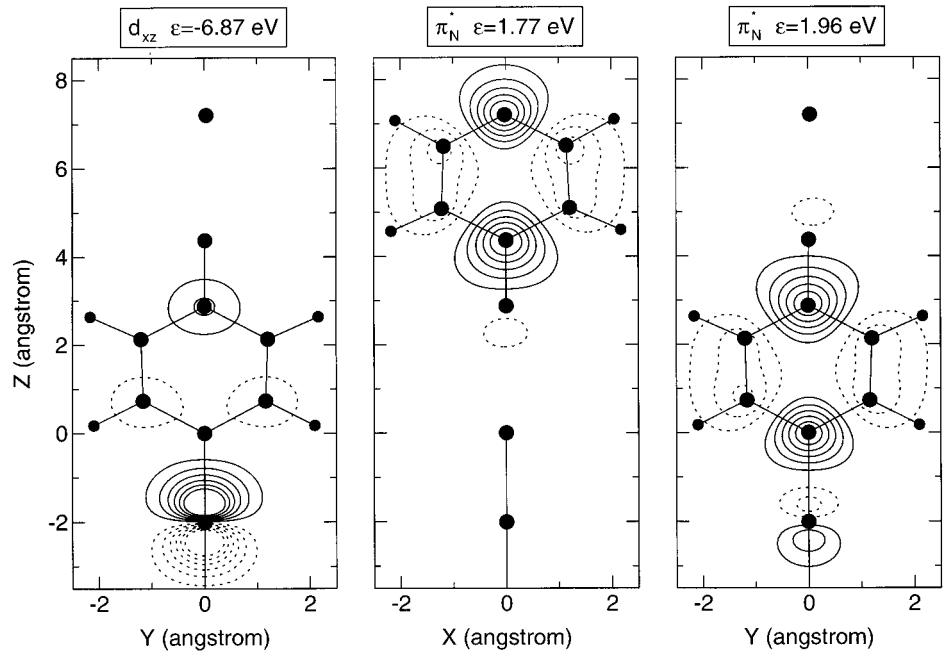

Figure 2. Maps of the low-lying orbitals at $\theta = 90°$ on the reported plane for the HOMO and the two N-based π^* orbitals (π_N^* in the figure). The value of the third coordinate is 0.6 Å.

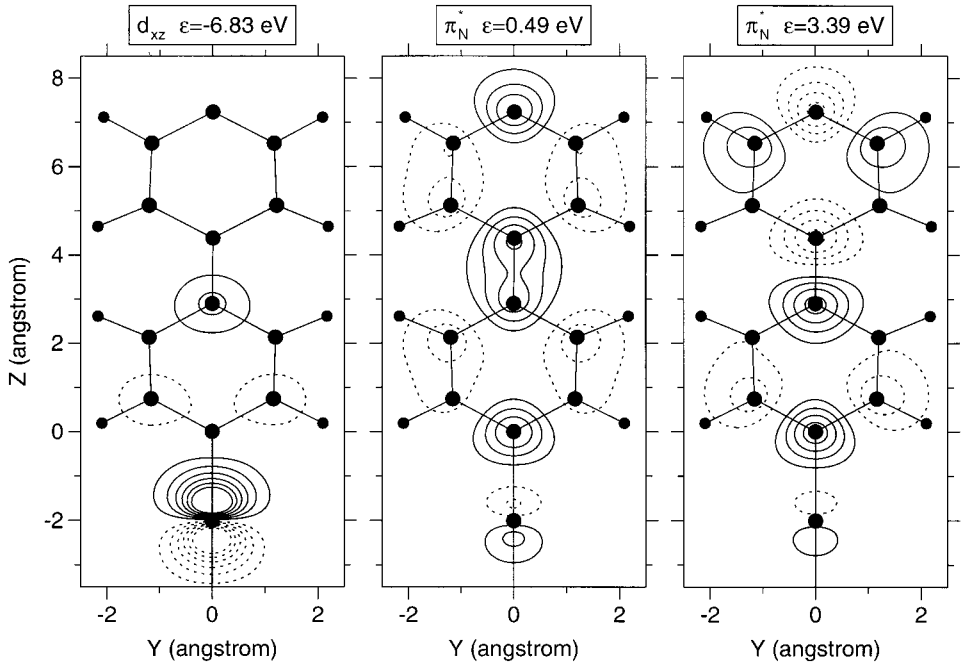

Figure 3. As for Figure 2 for $\theta = 0°$.

ring far from Ru, and the next orbital is that close to Ru, slightly mixed with the Ru d_{xz}. The Ru−pyr interaction makes the π^* on the ring nearest the metal slightly higher in energy than that on the farthest. When the two rings are on the same plane ($\theta = 0°$; Figure 3), the two pyr π^* are mixed. While the HOMO is practically unchanged, the LUMO is the bonding (symmetric) combination of the π^*'s on the two rings, and after two further π^* orbitals having a nodal plane coincident with the *xz* symmetry plane, there is the antibonding (antisymmetric) combination of the two.

The geometry relaxation of the aromatic ligand, performed for several values of the torsion, shows an overall decrease of the ground-state energy in the range 2 ± 0.25 kcal/mol. Thus, both the position of the minimum and the barrier heights (0° and 90°) are only slightly modified by the geometry relaxation.

The DFT energy curve is reported in Figure 4, where we also show the curves obtained by SCF, CI-V, and CI-VP calculations in vacuo. All curves have been shifted with respect to the energy at $\theta = 0°$. SCF computations predict a minimum at ∼40° and about the same barrier height for 0 and 90°. By comparison of these results with the SCF data reported in the literature for the 4,4′-bpy alone,[29,30] it appears that the position of the minimum is not significantly changed in the Ru compound (48−50° in the ligand alone), while relevant differences in the torsional barriers height are evident. For the isolated ligand a ∼4 kcal/mol barrier at 0° and a ∼1 kcal/mol barrier at 90° where found,[29] while in the Ru compound the barrier is roughly the same both at 0° and at 90°. This can be reasonably explained invoking Ru−pyr back-bonding that stabilizes the 0° with respect to the 90° geometry (at 90° the π^*'s on the two

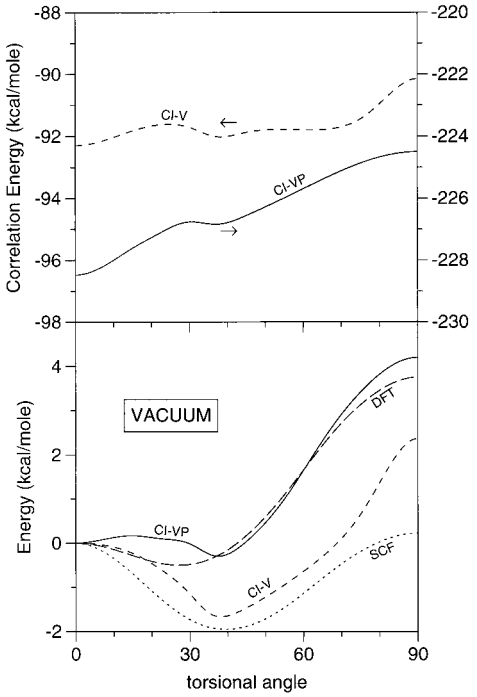

Figure 4. Ground-state energy in vacuo as a function of the torsion (θ) for the various kinds of calculation. Correlation energy as a function of θ in CI-V (left scale) and CI-VP (right scale) calculations (upper part).

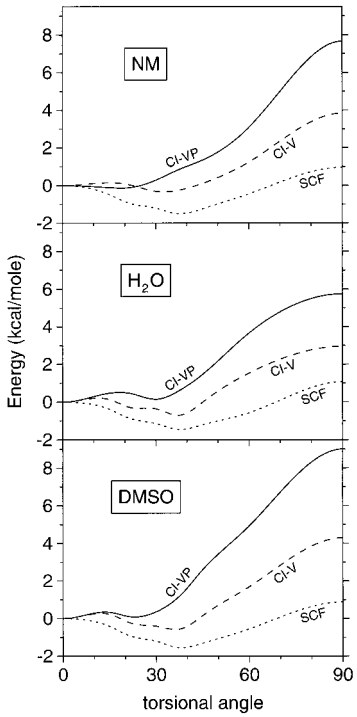

Figure 5. Ground-state energy in solution as a function of the torsional angle (θ) for the various calculations.

rings do not mix and the electronic charge cannot be delocalized). The inclusion of correlation effects by means of CI calculations changes substantially the ground-state energy dependence on θ. The variational results show that although the position of the minimum is unchanged and the barrier at $\theta = 0°$ only slightly decreases in comparison with SCF calculations, the barrier at 90° increases by about 2 kcal/mol. Such an increase is about twice (∼4 kcal/mol) in CI-VP calculations, where the depth of the minimum with respect to 0° decreases. This emphasizes the importance of the correlation energy (Figure 4a), which, besides being much higher in CI-VP than in CI-V calculations, shows a marked dependence on θ. This quantity monotonically increases (in absolute value) going from a perpendicular to a planar conformation of the two pyr rings. A simple explanation may be found in the HOMO−LUMO energy gap (see Figures 2 and 3), which grows with θ, and in the slight increase of electronic charge on bpy at low values of θ, due to a more effective Ru−bpy back-bonding. It is worthwhile to note that the CI-VP curve closely resembles the DFT one (within 0.7 kcal/mol), which includes also the correlation of the core orbitals. This agreement is a clear indication that our choice of the active orbitals and the correlation treatment in the CI-VP calculation is well equilibrated as far as the dependence on the torsional angle is concerned. For all these reasons we believe that the CI-VP results are the best among all those presented and their accuracy is sufficient to guarantee their use as predictive results.

The inclusion of solvent effects by the PCM method, together with our criterion for the choice of the cavity, gives the ground-state curves of Figure 5 in the three solvents considered. In solution, as in vacuo, the planar conformation is clearly the favorite and the correlation energy is again responsible for the high barrier at 90°. Its magnitude depends on the solvent donor number (DN),[31] but this dependence is not monotonic and the barrier is first seen to decrease, going from NM to water, and then to increase, going from water to DMSO, where it is the largest (∼9 kcal/mol). We do not have a simple explanation for this effect, which is clearly due to a different correlation energy in the various solvents, since SCF results are nearly the same in all three solvents.

Comparing the results of Figure 5 with those in vacuo of Figure 4, one may note that all solvents cause an increase of the barrier at 90°. Again, an explanation can be found in the enhancement of the metal-to-ligand back-bonding interaction, induced by the increased donor capabilities of the five ammonia ligands (see also ref 9). This partially populates the π^* orbital, thus increasing the electronic charge on both rings and enforcing the C−C (ring−ring) bond by a net π contribution. For instance, the Mulliken gross charges on the second ring is found to be +0.16, −0.02, −0.08, and −0.11 at 0° and +0.14, 0.00, −0.03, and −0.04 at 90° in vacuo, NM, H_2O, and DMSO, respectively. In the same sequence the Ru−N(pyr) bond index is found to be 0.54, 0.60, 0.65, and 0.68 at 0°, revealing that as DN increases, back-bonding increases as well, and at 0° it also affects the π distribution on the second ring. Since the SCF curves show a near-degeneration of the 0° and 90° conformations, it appears that this solvent effect tends to favor a planar conformation only if the electronic correlation is properly taken into account, as in CI-VP calculations.

A further remark can be made concerning the dependence of the ground-state energy on the torsion. Since in the range 0−40° the energy changes no more than 1 kcal/mol, the whole range is expected to be statistically populated at room temperature ($k_BT \approx 0.6$ kcal/mol), while the 90° conformation is strongly disfavored. This prediction is confirmed by the quantum statistical distribution function

$$P_Q(\theta) = \frac{\sum_j |\chi_{j0}(\theta)|^2 \, e^{-E_{j0}/(k_B T)}}{Z_Q} \qquad (7)$$

whose behavior at $T = 273.15$ K is reported in Figure 6 for all

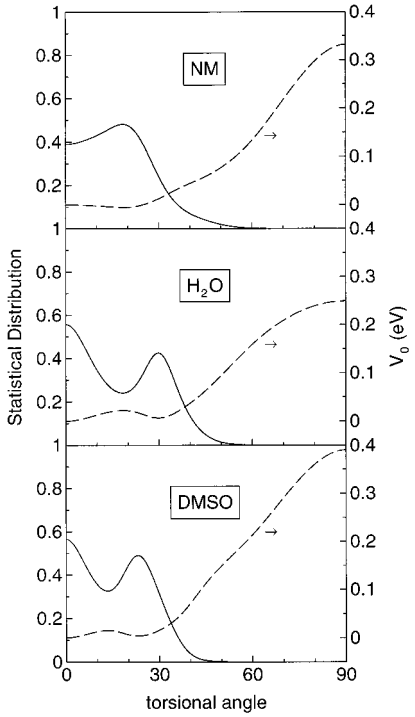

Figure 6. Ground-state population distribution (P_Q) as a function of θ in the three solvents (left scale, full line). The shifted energies of Figure 5 are also reported for a better understanding (right scale, dashed line).

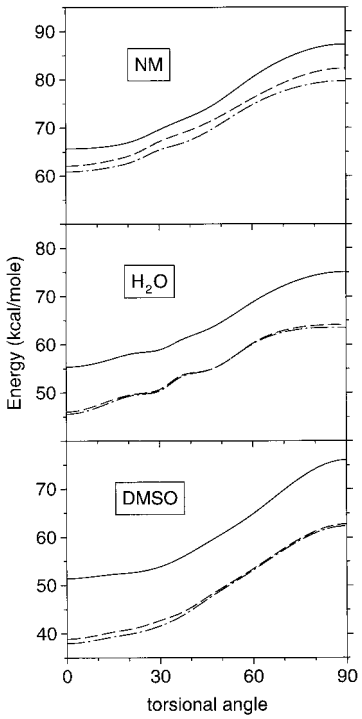

Figure 7. Energy curves of the lowest singlet excited states as a function of the torsion in the three solvents: continuous line is the $d_{xz} \rightarrow \pi^*$, dashed line is the $d_{x^2-y^2} \rightarrow \pi^*$, and dashed−dotted line is the $d_{yz} \rightarrow \pi^*$. The curves are shifted with respect to the ground-state energy at $\theta = 0°$ ($V_0(0)$).

the three solvents and referenced to the CI-VP ground-state energies of Figure 5.

In Figure 7 we show the energy curves of the first three excited states in solution as a function of the torsion, shifted by the corresponding ground-state energy at $\theta = 0°$ ($V_a(\theta) - V_0(0)$), while in Figure 8 the corresponding excitation energies

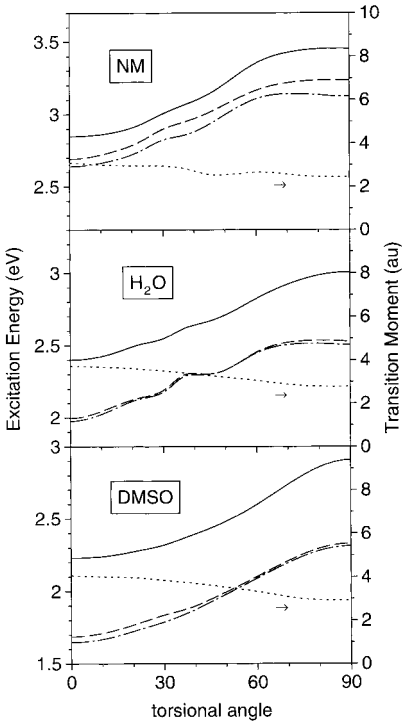

Figure 8. Excitation energies ($V_a(\theta) - V_0(\theta)$) as a function of the torsion in the three solvents (left scale): continuous line is the $d_{xz} \rightarrow \pi^*$, dashed line is the $d_{x^2-y^2} \rightarrow \pi^*$, and dashed−dotted line is the $d_{yz} \rightarrow \pi^*$. Electronic transition moment (dotted line, right scale) for the $d_{xz} \rightarrow \pi^*$ transition is also reported.

are reported ($V_a(\theta) - V_0(\theta)$). The continuous line corresponds to the strongest MLCT excitation in which one electron is promoted from the Ru d_{xz} (HOMO) to the lowest combination of the pyr π^* (LUMO). The two further curves are excitations from the two remaining near-degenerate t_{2g} orbitals to the same π^* and have small oscillator strength.

The excitation energy for all transitions decreases monotonically with DN; the solvent enforces the electron donor capability of the ammonia, causing an energy rise of the metal outer d orbitals.[9] Furthermore, the energy gap between the $d_{xz} \rightarrow \pi^*$ and the two near-degenerate $d_{yz} \rightarrow \pi^*$ and $d_{x^2-y^2} \rightarrow \pi^*$ curves grows with DN as a result of the corresponding increase of the $d_{xz}-\pi^*$ interaction.[9]

As already noted and explained in refs 9 and 14, although the $\pi-d_{xz}$ interaction causes the d_{xz} be the HOMO, at the same time the $d_{xz} \rightarrow \pi^*$ excitation energy is found to be greater than that from the two other d orbitals. This is due to the exchange integral $[d,\pi^*|d,\pi^*]$, which is small for the d_{yz} and $d_{x^2-y^2}$ orbitals and significant for the d_{xz}.

The barrier at 90° is much higher in the excited states than in the ground, and this can be easily understood in terms of the LUMO population that has a bonding character between the two rings.

Finally, in Figure 9 we show the absorption cross section (eqs 4 and 5) for the system under study in the three solvents. The discrete absorption lines are convoluted with a Gaussian function of fwhm = 0.1 eV (see previous section). The band maximum, which is found at 2.26, 2.42, and 2.88 eV in DMSO, H_2O, and NM, respectively, in reverse order with respect to DN (see also ref 9), is close to the vertical excitation energy at $\theta = 0°$ (see Figure 9). This is in accordance with the favorable conformation for low values of the torsion in both ground and excited electronic states. In the same Figure 9 we also report the statistically weighted oscillator strengths (eq 5) between the

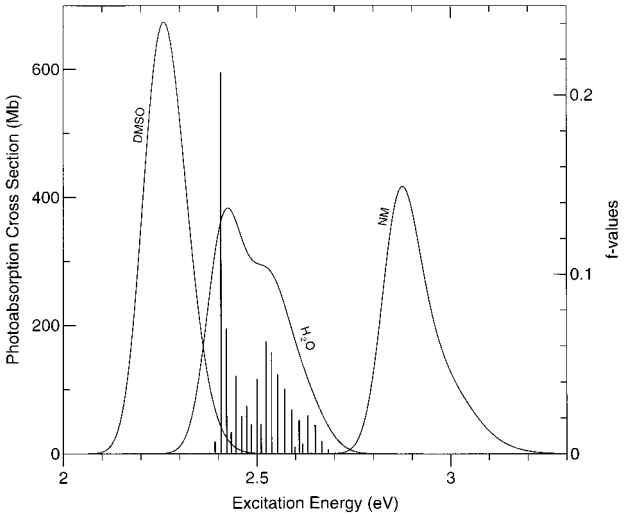

Figure 9. MLCT band in the three solvents (left scale). Vertical bars, only reported for water, are the oscillator strengths between vibronic states (right scale) computed by weighting with the Boltzmann equilibrium distribution.

discrete levels of the torsional states for H_2O (in NM and DMSO similar features are presents). While the more intense peak corresponds to the 0−0 transition, vibronic lines are spread over a range of about $10k_BT$ ($k_BT \approx 0.025$ eV).

As far as the line shape profile is concerned, the results of Figure 9, which only include the torsion among the many nuclear degrees of freedom that could be of relevance, we can conclude that as the solvent DN increases, the line shape becomes more symmetric (e.g., compare the band for NM with that for DMSO). However, the width of the band is not monotonic with DN (the largest is in water). Both these results can be interpreted in terms of the dependence of the ground-state energy on the torsion. In fact, as θ increases, the rise of the ground-state energy follows the order DMSO, NM, and H_2O, giving rise to a statistical population distribution on θ (see Figure 6) whose width grows in the same order. The oscillation of $V_0(\theta)$ for small values of the torsion is at the origin of the observed line shape profile. For NM this oscillation is almost absent and the profile is then close to the progression of Franck−Condon factors for undisplaced oscillators, while for water and DMSO the oscillation causes the profile to become similar to that of displaced oscillators.

A final remark can be made regarding the comparison with experimental results. While for pyrazine[9] the wide availability of experimental data[16] made possible a good comparison between computed excitation energies and measured absorption spectra in various solvents, for the present case there is only one result reported in water by Creutz et al.[17] The authors find an MLCT band with the maximum at 2.58 eV, a value that is in good agreement with the results of our computations.

Conclusions

We have reported a study of the absorption spectrum of the complex $[Ru(NH_3)_5-(4,4'\text{-bpy})]^{2+}$ in the visible, carried out by extensive CI calculations in which the solvent is introduced by the PCM model. This method, widely applied to the study of several physicochemical problems in solution, can be successfully applied to the study of absorption processes. When the formation of hydrogen bonds is the main source of solute−solvent interactions and the orbitals involved in the excitation are far enough from the solute−solvent interface, as in the case studied here, a suitable choice of the cavity guarantees a proper inclusion of solvent effects.

The dependence on the torsional angle θ of the ground and the lowest excited states has been studied in vacuum and in three solvents (nitromethane, water, and dimethylsulfoxide). Furthermore, the MLCT band profile has been computed including the torsional degrees of freedom.

The solvent effect found in the MLCT excitation of $[Ru(NH_3)_5-(4,4'\text{-bpy})]^{2+}$ has the same trend found experimentally for all Ru(II) complexes with N−aromatic ligands and, in particular, in the pyz compound.[16] As the solvent DN increases, the MLCT transition is red-shifted as a consequence of the increased electron density on Ru that lowers the HOMO−LUMO energy gap.[9] Note that DN and the dielectric constant are not linearly dependent.

Our results are in agreement with the only experimental result available, that in water by Creutz et al.[17]

The next step will now be that of attacking the dimer compound $[Ru(NH_3)_5-(4,4'\text{-bpy})-Ru(NH_3)_5]^{m+}$ ($m = 4$, 5, and 6), with the aim of getting a definitive answer on the nature of the observed near-IR−visible bands at various total charges m.

Acknowledgment. The authors acknowledge the help of Prof. Carol Creutz (Brookhaven National Laboratory) in collecting available experimental results, as well as fruitful discussion with Dr. Roberto Improta (ICQEM-CNR).

References and Notes

(1) Balzani, V.; Scandola, F. *Supramolecular Photochemistry*; Horwood: Chichester, U.K., 1991.
(2) Crutchley, R. J. *Adv. Inorg. Chem.* **1994**, *41*, 273.
(3) Hanack, M.; Lang, M. *Adv. Mater.* **1994**, *6*, 819.
(4) Ferretti, A.; Lami, A.; Villani, G. *J. Phys. Chem. A* **1997**, *101*, 9439.
(5) Ferretti, A.; Lami, A. *Chem. Phys.* **1994**, *181*, 107. Ferretti, A.; Lami, A. *Chem. Phys. Lett.* **1994**, *220*, 327.
(6) Ferretti, A.; Lami, A.; Villani, G. *Inorg. Chem.* **1998**, *37*, 2799, 4460.
(7) Murga, L. F.; Ferretti, A.; Lami, A.; Ondrechen, M. J.; Villani, G. *Inorg. Chem. Commun.* **1998**, *1*, 137.
(8) Ferretti, A.; Lami, A.; Murga, L. F.; Shehadi, I. A.; Ondrechen, M. J.; Villani, G. *J. Am. Chem. Soc.* **1999**, *121*, 2594.
(9) Cacelli, I.; Ferretti, A. *J. Chem. Phys.* **1998**, *109*, 8583.
(10) Oh, D. H.; Sano, M.; Boxer, S. G. *J. Am. Chem. Soc.* **1991**, *113*, 6880.
(11) Doorn, S. K.; Hupp, J. T.; Porterfield, D. R.; Campion, A.; Chase, D. B. *J. Am. Chem. Soc.* **1990**, *112*, 4999.
(12) (a)Tomasi, J.; Persico, M. *Chem. Rev.* **1994**, *94*, 2027. (b)Tomasi, J.; Mennucci, B.; Cammi, R.; Cossi, M. In *Computational Approaches to Biochemical Reactivity*; Nárayt-Szabó, G., Warshel, A., Eds.; Kluwer: Amsterdam, 1997; pp 1−102.
(13) (a) Zeng, J.; Hush, N. S.; Reimers, J. R. *J. Am. Chem. Soc.* **1996**, *118*, 2059. (b) Zeng, J.; Hush, N. S.; Reimers, J. R. *J. Phys. Chem.* **1996**, *100*, 19292.
(14) Shin, Y. K.; Brunschwig, B. S.; Creutz, C.; Newton, M. D.; Sutin, N. *J. Phys. Chem.* **1996**, *100*, 1104.
(15) Sizova, O. V.; Baranovski, V. I.; Ivanova, N. V.; Panin, A. I. *Int. J. Quantum Chem.* **1997**, *63*, 853.
(16) Creutz, C.; Chou, M. H. *Inorg. Chem.* **1987**, *26*, 2995.
(17) Winkler, J. R.; Netzel, T. L.; Creutz, C.; Sutin, N. *J. Am. Chem. Soc.* **1987**, *109*, 2381.
(18) Curtis, J. C.; Sullivan, B. P.; Meyer, T. J. *Inorg. Chem.* **1983**, *22*, 224.
(19) Hupp, J. T.; Meyer, T. J. *Inorg. Chem.* **1987**, *26*, 2332.
(20) Onsager, L. *J. Am. Chem. Soc.* **1936**, *58*, 1486.
(21) Mennucci, B.; Tomasi, J. *J. Chem. Phys.* **1997**, *106*, 5151.
(22) Lee, S.; Hynes, J. T. *J. Chem. Phys.* **1988**, *88*, 6853.
(23) Kim, H. J.; Hynes, J. T. *J. Chem. Phys.* **1990**, *93*, 5194.
(24) Aguilar, M. A.; Olivares del Valle, J.; Tomasi, J. *J. Chem. Phys.* **1993**, *98*, 7375.
(25) Cammi, R.; Tomasi, J. *Int. J. Quantum Chem.* **1995**, *29*, 465.
(26) (a) Becke, A. D. *J. Chem. Phys.* **1993**, *98*, 5648. (b) Frisch, M. J.; Trucks, G. W.; Schlegel, H. B.; Gill, P. M. W.; Johnson, B. G.; Robb, M.

A.; Cheeseman, J. R.; Keith, T. A.; Petersson, G. A.; Montgomery, J. A.; Raghavachari, K.; Al-Laham, M. A.; Zakrzewski, V. G.; Ortiz, J. V.; Foresman, J. B.; Cioslowski, J.; Stefanov, B. B.; Nanayakkara, A.; Challacombe, M.; Peng, C. Y.; Ayala, P. Y.; Chen, W.; Wong, M. W.; Andres, J. L.; Replogle, E. S.; Gomperts, R.; Martin, R. L.; Fox, D. J.; Binkley, J. S.; Defrees, D. J.; Baker, J.; Stewart, J. P.; Head-Gordon, M.; Gonzales, C.; Pople, J. A. *Gaussian 94*, revision E.1; Gaussian Inc.: Pittsburgh, PA, 1995.

(27) Hay, P. J.; Wadt, W. R. *J. Chem. Phys.* **1985**, *82*, 270, 284, 299.

(28) (a) Cimiraglia, R. *J. Chem. Phys.* **1985**, *83*, 1746. (b) Angeli, C.; Cimiraglia, R.; Persico, M.; Toniolo, A. *Theor. Chem. Acc.* **1997**, *98*, 57. (c) Angeli, C.; Persico, M. *Theor. Chem. Acc.* **1997**, *98*, 117.

(29) Ribeiro da Silva, M. A. V.; Morais, V. M. F.; Matos, M. A. R.; Rio, C. M. A. *J. Org. Chem.* **1995**, *60*, 5291.

(30) Ould-Moussa, L.; Poizat, O.; Castellà-Ventura, M.; Buntinx, G.; Kassab, E. *J. Phys. Chem.* **1996**, *100*, 2072.

(31) Gutmann, V. *The donor−acceptor approach to molecular interactions*; Plenum: New York, 1978; p 19.